Leadership, Education, Personality: An Interdisciplinary Journal ISSN: 2524-6178
www.sibe.rpress.co.in, Vol. 18, Issue 12 November 2023, UGC CARE 1

Influence of Ion Incidence Angle on the Implantation Characteristics of 60 keV Oxygen Ions in Aluminium: A SRIM/TRIM Simulation Study

S. S. Patil
Department of Physics, K. M. Agrawal College of Arts, Commerce and Science, Kalyan (W), Maharashtra, India
E-mail: pratinjay7668@gmail.com

Abstract
The implantation geometry of energetic ions controls penetration depth, reflection and collision-cascade morphology. Here, the influence of incidence angle on 60 keV oxygen-ion implantation into aluminium was evaluated using the Monte Carlo Binary Collision Approximation implemented in SRIM/TRIM. At each angle (6°, 12°, 18°, 24° and 30°, measured from the surface normal), 100,000 incident ions were simulated using a displacement energy of 25 eV, lattice binding energy of 3 eV and surface binding energy of 3.36 eV. Increasing the angle from 6° to 30° reduced the longitudinal projected range from 120.6 to 105.7 nm (12.35%) and increased backscattered ions from 391 to 998 (155.24%), corresponding to backscattering fractions of 0.391% and 0.998%. In contrast, the lateral projected range increased from 35.1 to 63.5 nm (80.91%), radial range from 53.9 to 77.2 nm (43.23%), lateral straggle from 43.8 to 73.3 nm (67.35%), and radial straggle from 27.5 to 34.4 nm (25.09%). Longitudinal straggle changed only from 39.8 to 39.4 nm, while vacancy production remained 315 vacancies per incident ion at every angle. The results show that increasingly oblique incidence produces a shallower but substantially broader near-surface affected volume and enhances reflection without changing the reported gross displacement yield. These findings provide a quantitative basis for selecting oxygen-implantation geometry in aluminium surface engineering, thin-film processing and oxide-layer design. Experimental depth profiling and phase analysis remain necessary before inferring retained oxygen concentration, alumina formation or property improvement.

Keywords: SRIM/TRIM; oxygen ion implantation; aluminium; incidence angle; projected range; straggling; backscattering; vacancy generation; Binary Collision Approximation; radiation damage.

1. Introduction

Ion implantation modifies the near-surface composition and defect structure of solids without requiring a deposited coating. The implanted depth, retained-ion distribution and radiation-damage field depend on ion mass, energy, target composition, displacement thresholds and beam geometry. In a collision-cascade description, energetic oxygen ions lose energy through interactions with target electrons and through elastic collisions with aluminium nuclei; the latter generate recoils and lattice displacements when the transferred energy exceeds the adopted displacement threshold [1–5].

Aluminium is widely used in aerospace structures, electrical conductors, microelectronic interconnects and lightweight engineering systems. Its native oxide provides passivation, while deliberately oxygen-enriched or alumina-containing surface layers can change hardness, friction, wear and electrical behaviour. Oxygen implantation of pure aluminium and aluminium-containing materials has produced nanoscale oxide precipitates or modified oxide layers under suitable fluence and temperature conditions [6–10]. Such chemical and functional outcomes remain dose-, temperature- and microstructure-dependent and cannot be inferred from range data alone.

Incidence angle is a useful processing variable because it changes the surface-normal component of motion and the likelihood of near-surface reflection. The present study quantifies the angle dependence of backscattering, vacancies, ranges and straggling for 60 keV O ions incident on Al at 6–30°. The objectives are to (i) compare depth and transverse cascade descriptors, (ii) quantify relative changes with angle, (iii) visualize the reported first moments and spread parameters in two and three dimensions, and (iv) distinguish conclusions supported by a static SRIM calculation from chemical or property claims requiring experimental validation.

2. Methodology: SRIM/TRIM simulation

2.1 Simulation design

The calculations used the Transport of Ions in Matter module of SRIM, a Monte Carlo code based on sequential binary collisions and semi-empirical stopping relations [5,11]. A monoenergetic 60 keV O beam was directed onto elemental Al at 6°, 12°, 18°, 24° and 30°. Throughout this paper, angle is defined relative to the surface normal. A total of 100,000 incident ions was used at every angle. The target parameters used for all runs were: displacement energy, 25 eV; lattice binding energy, 3 eV; and surface binding energy, 3.36 eV. The SRIM version/build, target density, layer thickness, calculation mode and all original input/output files should be reported or archived for submission.

2.2 Extracted quantities and analysis

The reported outputs were the number of backscattered ions, vacancies per incident ion, longitudinal projected range, longitudinal straggle, lateral projected range and straggle, and radial range and straggle. Lengths were converted from ångström to nanometres using 1 Å = 0.1 nm. The backscattering fraction was calculated as Nbs/100,000. Relative change was calculated as $100[X(30°)-X(6°)]/X(6°)$. No inferential uncertainty was supplied by the exported dataset; accordingly, the discussion treats the values as simulation estimates rather than experimentally measured quantities.

3. Theoretical background

3.1 Nuclear and electronic energy loss

The stopping power may be written as $-dE/dx = S_n(E)+S_e(E)$, where Sn is nuclear stopping and Se is electronic stopping. Elastic nuclear encounters transfer kinetic energy to Zr atoms and can initiate recoil cascades. Electronic stopping represents inelastic energy transfer to the target electron system. At each binary encounter, scattering is evaluated using a screened interatomic potential; repeated stochastic events generate a distribution of terminal positions rather than a single range [1,4,5].

3.2 Range, straggling and angular geometry

The longitudinal projected range Rp is the mean penetration component along the chosen depth direction, while longitudinal straggle ΔRp characterizes its statistical spread. Lateral and radial measures describe transverse dispersion. With increasing tilt from the surface normal, the normal component of a nominal straight trajectory scales approximately with $\cos\theta$; real trajectories additionally undergo multiple scattering. Therefore, a reduction in normal projected range can coexist with increased transverse spread and backscattering. The approximation is qualitative because collision trajectories are neither straight nor identical.

3.3 Vacancy estimate

A vacancy is counted when the recoil-transfer sequence satisfies the displacement criterion used by the code. The resulting vacancies-per-ion value is a prompt displacement estimate. It is not the surviving defect concentration after recombination, thermal diffusion, dynamic annealing, cascade overlap or dose accumulation. The classical NRT framework and later assessments emphasize that displacement counts are model quantities whose relationship to stable defects depends on material and irradiation conditions [3,4,12].

3.4 Basis of the 2D and 3D imaging

Because raw ion-coordinate and recoil-coordinate files were not provided, an authentic SRIM trajectory image or three-dimensional collision-cascade cloud cannot be reconstructed. For visualization only, the depth distribution at each angle was represented by a normalized Gaussian $p(z,\theta) = \exp\{-[z-R_p(\theta)]^2/[2\Delta R_p(\theta)^2]\}$, using linear interpolation between the reported Rp and ΔRp values. The resulting 2D contour and 3D surface preserve the supplied mean depth and longitudinal spread, but they do not constitute additional SRIM output, a concentration profile, or a prediction of retained dose.

4. Results and discussion

Table 1. Numerical results: Angle-dependent SRIM outputs for 60 keV O ions in Al. Lengths were converted from Å to nm; backscatter percentages assume 100,000 incident ions per run.

Angle (°)	Backscattered ions	Backscatter (%)	Vacancies/ion	Long. range (nm)	Long. straggle (nm)	Lateral range (nm)	Lateral straggle (nm)	Radial range (nm)	Radial straggle (nm)
6	391	0.391	315.0	120.6	39.8	35.1	43.8	53.9	27.5
12	461	0.461	315.0	118.6	39.7	39.5	48.8	57.4	28.9
18	542	0.542	315.0	115.6	39.6	46.2	56.1	62.8	32.8
24	690	0.690	315.0	110.9	39.6	54.4	66.1	69.6	32.6
30	998	0.998	315.0	105.7	39.4	63.5	73.3	77.2	34.4

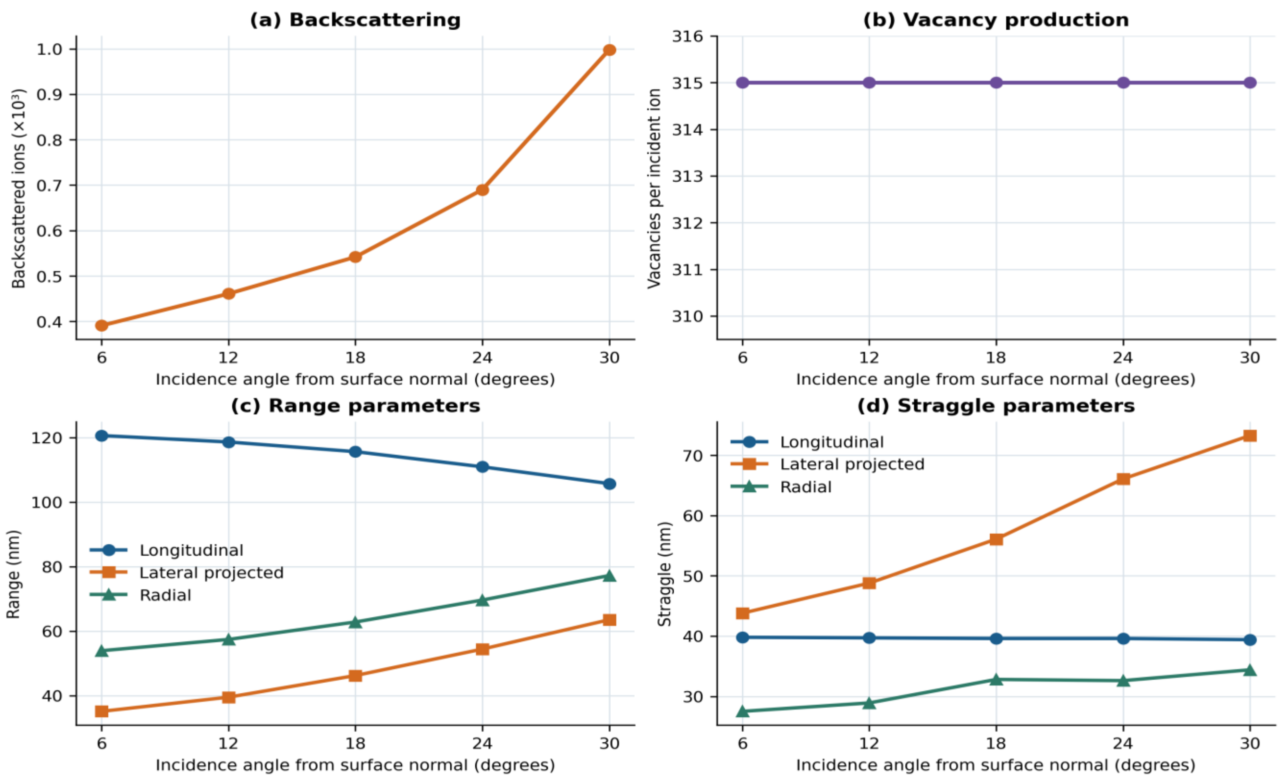

Figure 1. Dependence of (a) backscattering, (b) vacancy yield, (c) range and (d) straggle parameters on incidence angle. Points are the supplied SRIM values; connecting lines guide the eye.

4.2 Backscattering and depth contraction

The number of backscattered ions increased monotonically from 391 at 6° to 998 at 30°, raising the reflected fraction from 0.391% to 0.998%. This is an absolute increase of 0.607 percentage points and a relative increase of 155.24%. Simultaneously, Rp decreased from 120.6 to 105.7 nm, a reduction of 14.9 nm or 12.35%. A simple geometric projection Rp(6°)cos30°/cos6° gives approximately 105.0 nm, close to the simulated 105.7 nm. This agreement shows that geometric projection captures the leading trend, while the residual difference reflects scattering, energy loss and selective loss of reflected trajectories.

4.3 Lateral and radial broadening

The depth contraction was accompanied by strong transverse broadening. The lateral projected range increased by 80.91% (35.1 to 63.5 nm) and its straggle increased by 67.35% (43.8 to 73.3 nm). Radial range and radial straggle increased by 43.23% and 25.09%, respectively. Thus, oblique incidence redistributes the implanted population and collision cascade: it becomes shallower in the surface-normal direction but much broader parallel to the surface. The nearly monotonic changes indicate that beam angle can be used to tune the geometry of the affected layer even at fixed ion energy.

4.4 Longitudinal straggle and vacancy production

Longitudinal straggle changed only from 39.8 nm at 6° to 39.4 nm at 30° (−1.01%), with an almost flat progression. Vacancy production was reported as exactly 315 vacancies per ion at every angle. Consequently, within the numerical resolution of the supplied outputs, angle changes where the cascade is distributed and how many ions escape but not the gross prompt displacement yield. The exact constancy should be checked in the original output files because rounded tabulation can conceal small variations; recoil and energy-partition files would be required to explain the detailed mechanism.

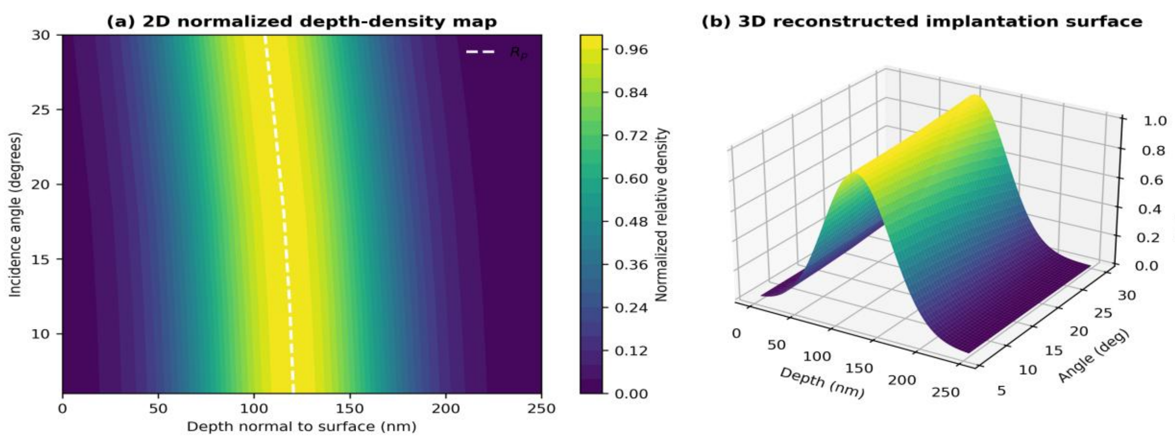

Figure 2. Data-derived imaging based on a normalised Gaussian reconstruction from the reported longitudinal range and straggle: (a) 2D depth–angle contour and (b) 3D surface. These are visualisations of first moments, not raw SRIM trajectories or absolute concentration maps.

4.5 Interpretation in relation to aluminium surface modification

The predicted mean depth scale (approximately 106–121 nm) places the implanted oxygen within a nanoscale surface region. Oxygen implantation studies on pure Al have reported alumina nanoprecipitates, enhanced hardness and reduced friction under suitable dose and temperature conditions, while low-energy irradiation has been used to create controlled aluminium-oxide layers [6–

9]. More recent oxygen implantation of Al-containing nanocomposites likewise demonstrates that implanted oxygen can modify surface structure and mechanical response [10]. The present simulation isolates angular transport at a fixed 60 keV energy; it does not establish Al2O3 formation, retained concentration, corrosion resistance or hardness because these require fluence, temperature, diffusion and chemical-state information.

4.6 Model limitations and reproducibility

Several constraints delimit the conclusions. Standard SRIM treats the target through an amorphous/random-collision approximation and does not explicitly reproduce crystallographic channeling, evolving Al-to-Al2O3 composition, dose-dependent sputter erosion, cascade overlap, defect recombination or long-time oxygen diffusion. Comparisons with experiment show that SRIM range estimates can exhibit material- and energy-dependent offsets [13]. Crystal-aware BCA or molecular-dynamics calculations are preferable when orientation and near-surface atomistic effects are central [14,15]. For reproducibility, the final submission should archive the SRIM version, input file, target density, layer thickness, calculation mode, random-seed policy and full outputs. Independent repeated runs would permit numerical confidence intervals.

5. Conclusions

A SRIM/TRIM study of 100,000 60 keV O ions incident on Al at 6°, 12°, 18°, 24° and 30° predicts a clear angular redistribution of ion transport. Between 6° and 30°, the longitudinal projected range decreases from 120.6 to 105.7 nm, while backscattering rises from 0.391% to 0.998%. The lateral projected range and lateral straggle rise by 80.91% and 67.35%, respectively; radial range and radial straggle increase by 43.23% and 25.09%. Oblique incidence therefore produces a shallower but substantially broader affected region. Vacancy production remains 315 vacancies per ion at every reported angle, so the angle dependence is much stronger for cascade geometry and reflection than for gross prompt displacement yield. The 2D and 3D reconstructions visualise the supplied range moments but are not raw trajectory images or absolute oxygen concentration maps. Experimental depth profiling, phase analysis and mechanical/corrosion tests are required to connect the predicted trends to alumina formation and functional properties.

Data availability and declaration
The numerical dataset analysed in this study is reproduced in Table 1. No external funding or conflict of interest was declared. This manuscript reports a computational study; no human participants, animals or biological samples were involved.

References

[1] J. Lindhard, M. Scharff, H. E. Schiøtt, Range concepts and heavy ion ranges, Mat. Fys. Medd. Dan. Vid. Selsk. 33(14) (1963) 1–42.

[2] G. H. Kinchin, R. S. Pease, The displacement of atoms in solids by radiation, Rep. Prog. Phys. 18 (1955) 1–51. https://doi.org/10.1088/0034-4885/18/1/301.

[3] M. T. Robinson, I. M. Torrens, Computer simulation of atomic-displacement cascades in solids in the binary-collision approximation, Phys. Rev. B 9 (1974) 5008–5024. https://doi.org/10.1103/PhysRevB.9.5008.

[4] M. J. Norgett, M. T. Robinson, I. M. Torrens, A proposed method of calculating displacement dose rates, Nucl. Eng. Des. 33 (1975) 50–54. https://doi.org/10.1016/0029-5493(75)90035-7.

[5] J. F. Ziegler, J. P. Biersack, U. Littmark, The Stopping and Range of Ions in Solids, Pergamon Press, New York, 1985.

[6] R. Günzel, E. Wieser, E. Richter, J. Steffen, Plasma source ion implantation of oxygen and nitrogen in aluminum, J. Vac. Sci. Technol. B 12 (1994) 927–930. https://doi.org/10.1116/1.587329.

[7] M. Bolduc, B. Terreault, A. Reguer, E. Shaffer, R. G. St-Jacques, Selective modification of the tribological properties of aluminum through temperature and dose control in oxygen plasma source ion implantation, J. Mater. Res. 18 (2003) 2779–2792. https://doi.org/10.1557/JMR.2003.0388.

[8] M. Bolduc, B. Terreault, E. Shaffer, Radiation-enhanced diffusion and improved tribological properties of aluminum co-implanted with O2+Ar, Surf. Coat. Technol. 186 (2004) 255–260. https://doi.org/10.1016/j.surfcoat.2004.04.032.

[9] K. E. Prikhodko, M. M. Dementyeva, B. A. Gurovich, D. A. Komarov, L. V. Kutuzov, Formation of high-quality aluminum oxide under ion beam irradiation, KnE Mater. Sci. 4 (2018) 1–8. https://doi.org/10.18502/kms.v4i1.2122.

[10] F. Sourani, M. H. Enayati, F. Ashrafizadeh, F. S. Sayyedan, P. K. Chu, Enhancing surface properties of (Fe,Cr)Al–Al2O3 nanocomposite by oxygen ion implantation, J. Alloys Compd. 853 (2021) 156892. https://doi.org/10.1016/j.jallcom.2020.156892.

[11] J. F. Ziegler, M. D. Ziegler, J. P. Biersack, SRIM – The stopping and range of ions in matter (2010), Nucl. Instrum. Methods Phys. Res. B 268 (2010) 1818–1823. https://doi.org/10.1016/j.nimb.2010.02.091.

[12] K. Nordlund, S. J. Zinkle, A. E. Sand, et al., Primary radiation damage: A review of current understanding and models, J. Nucl. Mater. 512 (2018) 450–479. https://doi.org/10.1016/j.jnucmat.2018.10.027.

[13] M. Titze, J. L. Pacheco, T. Byers, S. B. Van Deusen, D. L. Perry, D. Weathers, E. S. Bielejec, Evaluation of the accuracy of stopping and range of ions in matter simulations through secondary ion mass spectrometry and Rutherford backscattering spectrometry for low energy heavy ion implantation, J. Vac. Sci. Technol. A 39 (2021) 063222. https://doi.org/10.1116/6.0001406.

[14] M. Posselt, Crystal-TRIM and its application to investigations on channeling effects during ion implantation, Radiat. Eff. Defects Solids 130–131 (1994) 87–119.

[15] L. Bukonte, F. Djurabekova, K. Nordlund, Comparison of molecular dynamics and binary collision approximation simulations for atom displacement analysis, Nucl. Instrum. Methods Phys. Res. B 297 (2013) 23–28. https://doi.org/10.1016/j.nimb.2012.12.014.